Light-Induced Currents at Domain Walls in Multiferroic $BiFeO_3$

Burak Guzelturk[1, 2 *], Antonio B. Mei[3], Lei Zhang[4], Liang Z. Tan[5], Patrick Donahue[4], Anisha G. Singh[6], Darrell G. Schlom[3], Lane W. Martin[4, 5], Aaron M. Lindenberg[1,2,7,8 *]

[1] Department of Materials Science and Engineering, Stanford University, Stanford, CA 94305, USA

[2] Stanford Institute for Materials and Energy Sciences, SLAC National Accelerator Laboratory, Menlo Park, CA, USA

[3] Department of Materials Science and Engineering and Kavli Institute at Cornell for Nanoscale Science, Cornell University, Ithaca, NY 14853, USA.

[4] Department of Materials Science and Engineering, University of California Berkeley, Berkeley CA 94720, USA

[5] Molecular Foundry, Lawrence Berkeley National Laboratory, Berkeley, CA 94720

[6] Department of Applied Physics, Stanford University, Stanford, CA, 94305, USA

[7] The PULSE Institute for Ultrafast Energy Science, SLAC National Accelerator Laboratory,
Menlo Park, CA, USA

[8] Department of Photon Science, Stanford University and SLAC National Accelerator Laboratory, Menlo Park, CA, USA

[*]Corresponding Authors: burakg@stanford.edu, aaronl@stanford.edu

Multiferroic $BiFeO_3$ (BFO) films with spontaneously formed periodic stripe domains can generate above-gap open circuit voltages under visible light illumination, nevertheless the underlying mechanism behind this intriguing optoelectronic response has not been understood to date. Here, we make contact-free measurements of light-induced currents in epitaxial BFO films via detecting terahertz radiation emanated by these currents, enabling a direct probe of the intrinsic charge separation mechanisms along with quantitative measurements of the current amplitudes and their directions. In the periodic stripe samples, we find that the net photocurrent is dominated by the charge separation across the domain walls, whereas in the monodomain samples the photovoltaic response arises from a bulk shift current associated with the noncentrosymmetry of the crystal. The peak current amplitude driven by the charge separation at the domain walls is found to be two orders of magnitude higher than the bulk shift current response, indicating the prominent role of domain walls acting as nanoscale junctions to efficiently separate photogenerated charges in the stripe domain BFO films. These findings show that domain-wall-engineered BFO thin films offer exciting prospects for ferroelectric-based optoelectronics, as well as bias-free strong terahertz emitters.

Keywords: Ferroelectrics, $BiFeO_3$, domain walls, photovoltaic effect, shift current, terahertz emission

Today, materials that enable efficient solar energy harvesting are under intensive research [1–6]. To this end, ferroelectrics have long attracted interest due to anomalous photovoltaic responses that were observed in prototypical systems such as $LiNbO_3$[7–9]. Recently, thin films of multiferroic oxide $BiFeO_3$ (BFO) with spontaneously formed stripe domains exhibited such a response reflected by open circuit voltages that are much larger than the band gap of the material[10–12]. This observation led to an ever-increasing interest in BFO thin films for wide range of optoelectronic applications, but the underlying mechanism behind this anomalous response in the stripe domain BFO films has remained puzzling. Early reports identified the critical role of domain walls (DWs) in optoelectronic response as evidenced by sample orientation dependent photovoltage measurements[10,11,13]. In agreement with this, Seidel *et al.* proposed that the DWs generate photovoltages

that are additive, hence DWs underlie the observed above gap open circuit voltages[11]. Nevertheless, other reports suggested dominant contributions of the bulk photovoltaic effects[12,14–16] inferred from excitation light polarization dependence of the measured photocurrents. Also, ref. [12] indicated a potential detrimental role of the DWs in photovoltage generation due to their large intrinsic conductivity which opposed the DW-mediated photovoltaic mechanisms[11]. Therefore, the individual contributions of different photovoltaic mechanisms in BFO films have not been disentangled and remain debated to date [3,4,17].

A common complication in prior experimental studies was that optoelectronic characterization was typically performed using devices with physical electrodes, where metal – ferroelectric interfaces can greatly modify photovoltaic response due to the formation of Schottky barriers[18,19], field screening and generation of interfacial defects[20]. For example, Pintilie *et al.* found that the photovoltaic response in ferroelectric Pb(Zr, Ti)O_3 varies with the choice of metal used as the top contact[19]. Although samples with Au and Ag contacts exhibited a bulk photovoltaic response, the ones using Pt and Cu exhibited a different one dominated by the band bending at the interface. This emphasizes the need for contact-free measurements of light-induced currents in photovoltaic ferroelectrics to extract and understand intrinsic physical phenomena. To this end, terahertz (THz) emission provides an all-optical means to measure light-induced currents, with the emitted fields directly arising from time-varying currents and their polarization state encoding the direction of the currents. This approach has been employed in prior studies to probe the initial steps of charge separation in semiconductor surfaces[21–24] and photo-induced currents in spintronic[25] and topological[26] systems. Furthermore, state-of-the-art THz detection systems offer high sensitivity and can detect electromagnetic radiation emitted by transient currents arising from charge separation across sub-nanometer thick two-dimensional heterointerfaces[27].

Here, we report the observation of broadband terahertz radiation emitted by epitaxial BFO films in the absence of external bias or prior electrical poling. By analyzing the polarization properties of the emitted THz fields, we find that the light-induced currents in periodic stripe-domain BFO samples exclusively flow perpendicular to the DWs, which emerges due to the dominant charge separation at

the domain walls. The DW-mediated spatially localized current dominates over other bulk photovoltaic current response. The DW-mediated current response is further confirmed by measurements as a function of domain-wall density, showing scaling with density. Samples with stripe domain structure grown via two different growth techniques exhibit the same response, hence DW-mediated charge separation is intrinsic to the periodic stripe BFO films and independent of growth technique. In the case of monodomain BFO, measurements supported with first principles modeling[14,16] indicate that the light-induced currents follow a shift current response. . Shift current is a bulk photovoltaic effect[28] that arises in noncentrosymmetric crystals when the evolution of excited electron and hole wavefunctions under a driving optical field is asymmetric[29,30], and has been shown to boost photovoltaic performance in energy-relevant materials[3132]. We find that the DW-mediated peak photocurrent is two orders of magnitude stronger as compared to that of the bulk shift current response. Thus, DW-mediated charge separation in the periodic stripe BFO films is substantially more efficient than bulk photovoltaic effects in BFO at room temperature.

We investigate THz emission from $BiFeO_3/SrRuO_3/DyScO_3$ $(110)_O$ films (see Figure 1a) in a reflection geometry with an oblique incidence excitation (Figure 1d and Figure S1). The subscript O denotes the orthorhombic indices of the $DyScO_3$ substrate in the non-standard *Pbmn* setting; these substrates are commonly used to achieve two domain variants in $BiFeO_3$ films separated by 71° domain walls[33]. There exists both a net in-plane and out-of-plane ferroelectric polarizations (see Figure 1b). Figure 1c shows a piezo force microscopy image of the stripe domains with the inset showing the in-plane polarizations in the domains. Above-band-gap 400 nm femtosecond pulses are used for excitation with the emitted THz fields and their polarization state detected using electro-optic sampling. Figure 2a shows the emitted THz transients (detecting only p-polarized THz fields) measured for two different azimuthal orientations of the sample (0° and 180°), where 0° means that the DWs lie along $+\hat{y}$, perpendicular to the *xz* plane of incidence of the 400 nm pulse (Figure 2a inset). In this orientation, the net in-plane polarization points along $-\hat{x}$. When the sample is azimuthally rotated by 180°, the polarity of the THz field completely flips (Figure 2a). This indicates that the transient current giving rise to

the emitted THz fields must be an in-plane current. The polarization state of the emitted THz field is further resolved with the help of two wire-grid THz polarizers (Figure S2). Figure 2b shows the THz transients measured for two orthogonal polarization states (p and s) when the sample is oriented 0° (top panel) and 90° (bottom panel). In both configurations, the radiated field is polarized perpendicular to the DWs with a negligible contribution (< 5%) parallel to the DWs. This observation indicates that the net current dominantly flows perpendicular to the DWs. Therefore, emission mechanisms such as surface band bending[21] and photo-Dember[22] effects, which would produce only net out-of-plane currents, can be ruled out. The absence of strong out-of-plane current despite the existence of net out-of-plane ferroelectric polarization implies that bulk photovoltaic response (e.g., shift current[16]) is significantly weaker as compared to the DW-mediated currents. Importantly, we find the direction of the net in-plane current by comparing the THz polarization to that of a well-known surface emitter (Fig. S3). In the orientation of 0°, the net current flows along $\hat{x}$. Therefore, net in-plane current is flows anti-parallel to the direction of the net in-plane ferroelectric polarization consistent with a screening response driven by the built-in fields at the DWs[11] (see Fig. 2d inset).

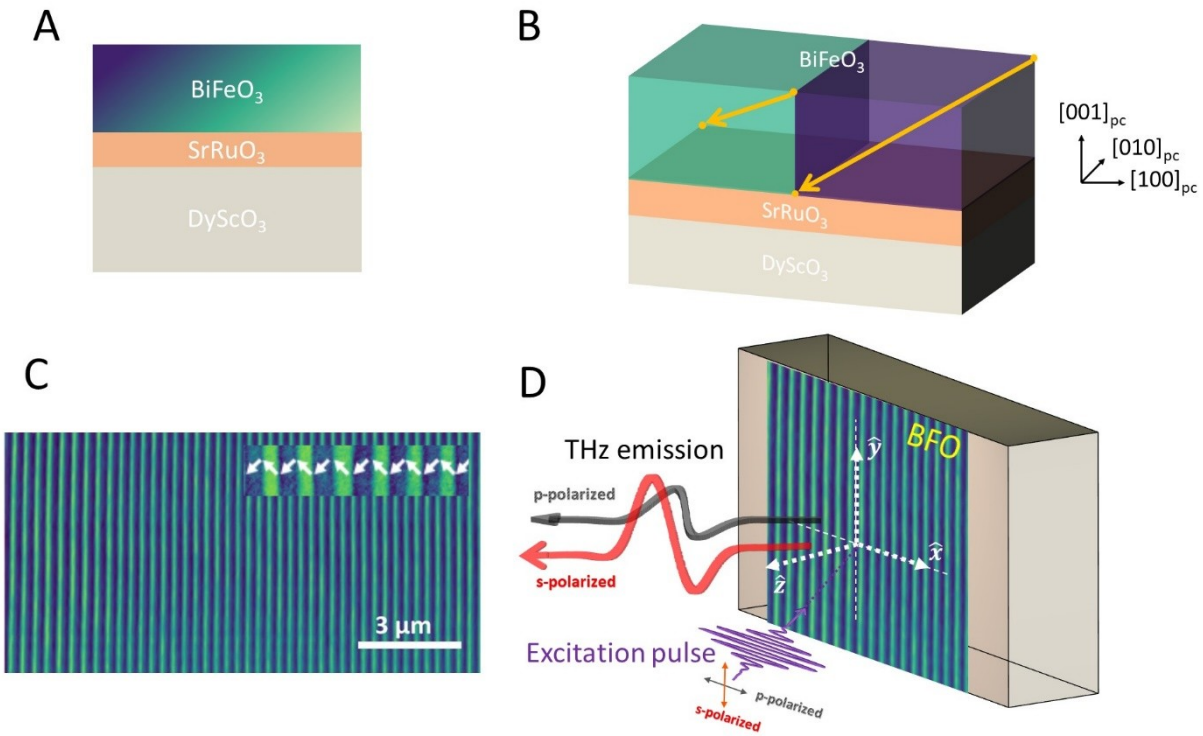

Figure 1. (a) Schematic shows film stack of the stripe domain BFO samples. (b) Spontaneous ferroelectric polarization direction (in-plane and out-of-plane) with respect to the crystal axes in the stripe domain samples with 71° domain walls. The samples exhibit net in-plane polarization along $[-100]_{pc}$. (c) Piezo force microscopy image of the periodic stripe domains. The inset shows the in-plane ferroelectric polarization components highlighted by white arrows. (d) Schematic shows the oblique incidence angle reflection mode configuration for the terahertz (THz) emission experiments. The emitted electromagnetic radiation is either p- or s-polarized. Crystal axes$[001]_{pc}$ and $[100]_{pc}$ point along $\hat{z}$ and $\hat{x}$, respectively.

Figure 2c shows the excitation light polarization dependence of the emitted THz radiation. As the half wave plate is rotated, the THz amplitude oscillates with a DC offset. This oscillatory behavior is completely captured by the Fresnel equations for an oblique incidence excitation considering the varying degree of reflection/transmission at the sample surface (Supp. Info.). This observation further supports the argument that the bulk photovoltaic effect is not dominant in the periodic stripe BFO sample, since this effect[28] would have led to a strong dependence on the excitation light polarization in addition to the Fresnel coefficients, which will be discussed for the monodomain sample below.

Figure 2d shows the fluence dependence of the THz emission, where the radiated THz field is observed to increase linearly within a large range from 0.1 to 100 $\mu J/cm^2$. THz emission does not show a saturation behavior within this range, thus charge separation at the DWs remains efficient even under high excitation density. It is important to note that an excitation fluence of 0.1 $\mu J/cm^2$ (~500 mW/cm^2) corresponds to a 5-sun-equivalent excitation (Supp. Info.), hence the currents resolved here are of relevance to the photovoltaic operation. The radiated THz field amplitude (E_{THz}) can be related to its transient source current by assuming a sheet current density ($J_{surface}$)[34]:

$$E_{THz} = \eta \times J_{surface} \times Z_0 \ , \qquad (1)$$

where η is the outcoupling factor, and Z_0 is the impedance of free space. We experimentally find E_{THz} = 24.4 V/cm under an excitation fluence of 30 $\mu J/cm^2$, and this field corresponds to an associated net $J_{surface}$ of 40 A/m. Using $J_{surface}$, the areal

coverage of the DWs (~1.5%) and the conductivity at THz range, we apply Ohm's low to estimate the built-in field (F_{DW}), which is 23.7 MV/m (see further details of the calculation in the Supp. Info.). The built-in field agrees well with our estimate (F_{DW} = 22 MV/m) using density functional theory for the 71° DWs (see Figure S7), and is in accordance with the previous theoretical prediction (F_{DW} = 40 MV/m)[11]. We further justify the built-in field at the DWs by considering a counter field that arises due to the screening of separated electron-hole pairs across a parallel plate: $E_{rev}=n/(\varepsilon¿¿0\varepsilon_r)¿$, where n is charge density across the DW. We estimate the counter field to be $E_{rev}=¿$ 24.1 MV/m under a fluence of 100 μJ/cm^2, where the emitted THz amplitude does not show a saturation (Figure 2d). Therefore, the built-in field F_{DW} must be equal or larger than the E_{rev}, corroborating the F_{DW} estimated above. As compared to the conventional photoconductive THz emitters, which are typically biased with an acceleration field of a few MV/m, the DWs in BFO films with periodic stripe-domains offer larger built-in acceleration fields at the nanoscale. Therefore, bias-free THz emitters based on stripe-domain BFO could offer comparable or even stronger THz amplitudes than those of state-of-the-art photoconductive THz emitters[35]. In comparison to conventional surface THz emitters (e.g., InSb), emitted THz amplitude from stripe domain BFO is smaller only by a factor of 5 under the same excitation condition. However, the domain walls only constitute ~1% of the BFO film, hence there is a large room to boost THz emission further with samples having higher densities of DWs. Figure S4 shows the spectrum of the emitted THz radiation from the stripe-domain samples, which has a bandwidth up to 7.5 THz that is limited by our electro-optic detection system. Therefore, bias-free THz emitters based on BFO films with periodic stripes would offer a complete spectral coverage of the THz band (0.1 – 10 THz).

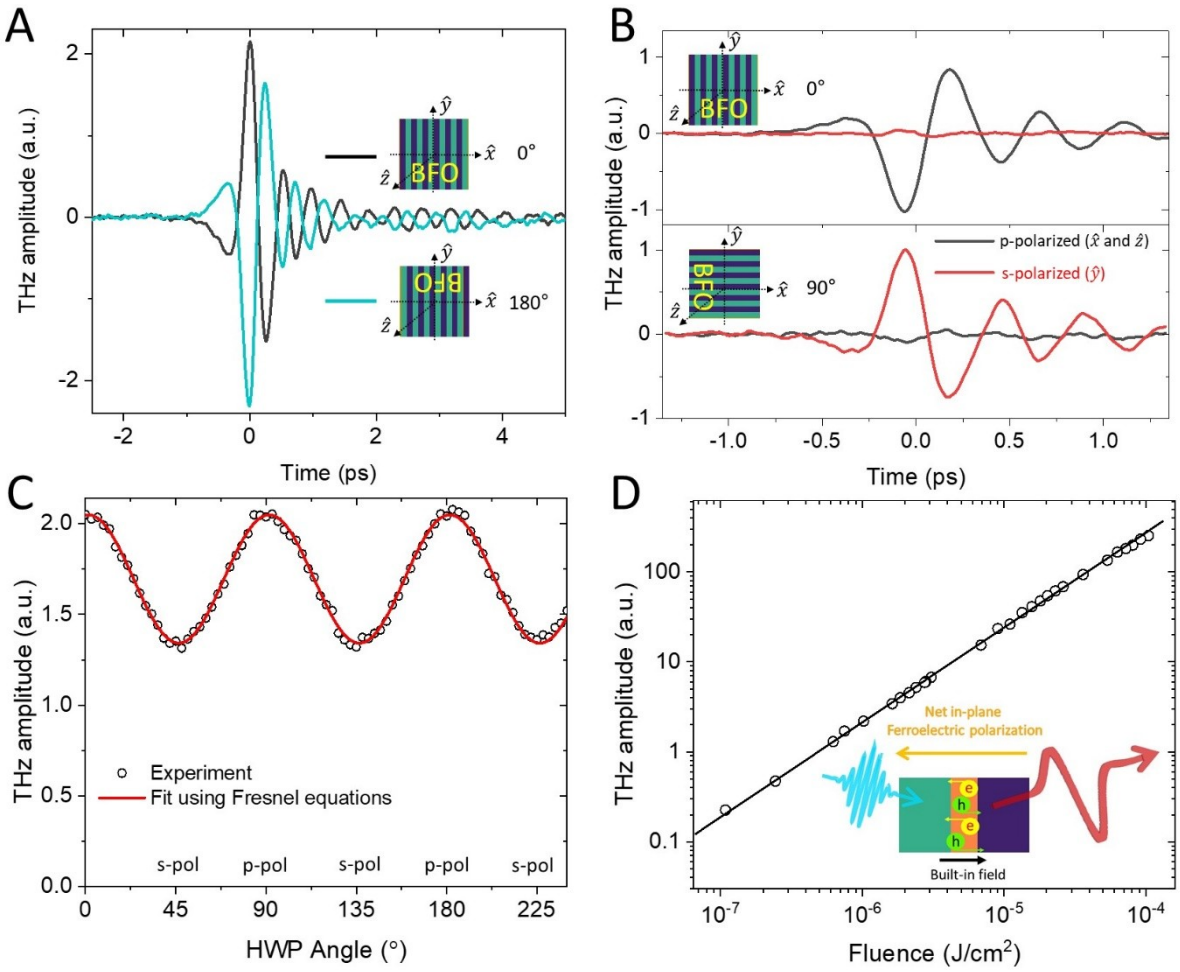

Figure 2. (a) Time-domain THz transients for the sample in 0° and 180° orientations, where 0° corresponds to the direction where DWs lie along $\hat{y}$. (b) Polarization-resolved THz transients for p- (black) and s-polarization (red) for the sample orientations of 0° (top) and 90° (bottom). (c) Excitation light polarization dependence of the THz emission (sample is oriented in 0°). The half wave plate (HWP) angle is varied while monitoring the peak THz amplitude. The fit is performed using the Fresnel equations to account for the polarization dependent reflection/transmission at the BFO surface. (d) Fluence dependence of the THz emission amplitude. The inset shows the THz emission mechanism in the periodic stripe domain sample which arises due to efficient charge separation across the domain walls due to the built-in electric field at the domain walls.

Figure 3 compares the THz field amplitudes emitted by three different periodic domain samples that were grown via two different methods (i.e., pulsed-laser

deposition[10] and molecular-beam epitaxy[36]). All of the samples consistently exhibit the DW-mediated response described above. The DW densities of the samples are 8.7, 7.7 and 6.9 DWs/μm (Figure S8 and Figure S9 for the PFM images of the samples) with thicknesses ranging from 70 to 220 nm. Importantly, increase in the DW density in stripe-domain BFO films leads to a larger THz field amplitude, and the amplitude exhibits a linear scaling the with DW density (see the insert of Figure 3) in support of the DW-mediated charge separation mechanism. Furthermore, Figure 3 shows the THz emission from a 100 nm thick monodomain (untwinned) BFO ($BiFeO_3/SrRuO_3/SrTiO_3$) in $(110)_{ps}$ (in pseudo-cubic notation for the BFO), which has 3.5-fold smaller amplitude as compared to the samples with periodic stripe domains, where all samples are in the orientation of 0° in Figure 3. Also, to note, none of the samples were poled prior to the measurements.

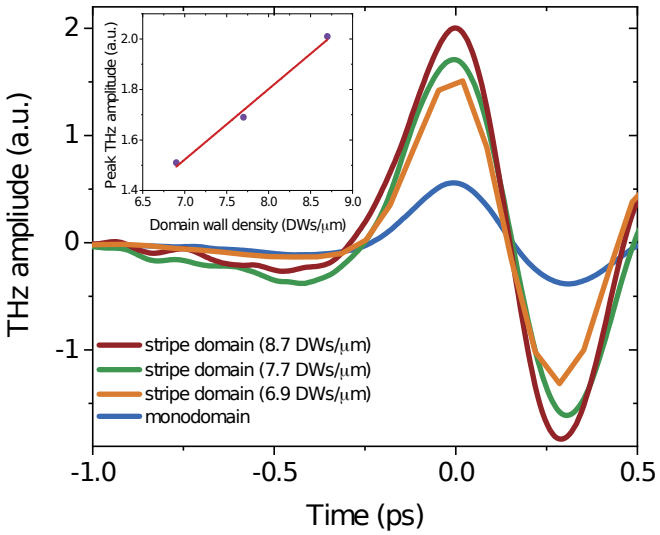

Figure 3. Radiated THz transients from three different stripe domain samples with 8.7 DWs/μm (red), 7.7 DWs/μm (green) and 6.9 DWs/μm (orange), and monodomain BFO sample (blue) under the same excitation condition. All the samples are in the orientation of 0° as described in the text. The inset shows the peak THz amplitude as a function of DW density exhibiting a linear scaling.

Previously, THz emission was observed in monodomain BFO films which were electrically poled prior to the measurements[37,38]. The THz emission, which was detected under surface normal excitation in a transmission geometry, was attributed to ultrafast depolarization of the ferroelectric polarization[37]. However,

other potential mechanisms such as the ones that arise from second order nonlinearities (e.g., shift current and optical rectification) associated with the intrinsic noncentrosymmetry of the BFO could not be ruled out since neither excitation light polarization dependence was investigated nor the out-of-plane currents were probed in the prior studies. To elucidate the emission mechanism in the monodomain BFO, THz transients are measured for different azimuthal orientations of the sample (0°, 90°, 180° and 270°) with the pump polarization first fixed as p-polarized (Figure 4a). Figure 4b shows the ferroelectric polarization in the monodomain sample exhibiting net in-plane and out-of-plane polarizations and Figure 4c shows the polarization directions for different sample orientations. The electro-optic sampling system is also fixed such that it is only sensitive for p-polarized THz radiation; therefore, we resolve net currents that flow along $\hat{x}$ and/or $\hat{z}$. Sample orientations of 90° and 270° exhibit the same signal amplitude without a polarity flip, which implies that the net current under these orientations must be out-of-plane. On the other hand, the orientations of 0° and 180° exhibit a polarity reversal, with 0° orientation exhibiting larger absolute amplitude than that of 180°. This observation can be explained with the co-existence of in-plane ($\hat{x}$) and out-of-plane $(\hat{z})$ currents projecting together onto a p-polarized emission, where the currents are additive for the orientation of 0°, but subtractive for the 180° orientation (see Figure 4c). By comparing the THz amplitudes measured under different orientations, we find that 65% (35%) of the THz emission stems from the in-plane (out-of-plane) currents in the orientation of 0°. In the 0° orientation, after decomposing the transient currents, net in-plane and out-of-plane currents point along $\hat{x}$ and $\hat{z}$ directions, respectively, which is antiparallel to the intrinsic ferroelectric polarization (Figure 4c). Figure 4d shows the excitation light polarization dependence of the emitted THz amplitude for the monodomain sample that is orientated at 90° (the same for 270°), where the THz emission arises only from an out-of-plane current. The modulation of the THz amplitude as a function of the half-wave plate angle cannot be fully captured by the Fresnel equations alone (see Figure S10), signifying that the emission is not directly associated with the number of photogenerated carriers. Therefore, this rules out the ultrafast depolarization of the ferroelectric polarization as the mechanism of the THz emission, which would only depend on the number of carriers created but not the

excitation light polarization. To account for the excitation light polarizations, we theoretically estimate the shift current response by considering the shift current tensor at 400 nm excitation under varying excitation polarization, and Figure S6 shows the predicted nonlinear conductivity for the in- and out-of-plane shift current components. As shown in Figure 4d, the out-of-plane shift current ($J_{[110]}^{shift}$) model excellently fits the excitation polarization dependence of the THz emission under the orientation of 90°, both for the modulation depth and the phase without any additional fit parameter needed. This observation strongly indicates that the THz emission in the monodomain BFO arises from a shift current response.

Moreover, we compare the amplitudes of the transient currents in the monodomain BFO and the calculated shift currents. The experimental $J_{surface}$ in the monodomain sample is calculated to be 9 A/m and 16 A/m for the in-plane and out-of-plane currents, respectively. The out-of-plane current amplitude is larger than the in-plane one but emitted THz for the in-plane current is stronger since the outcoupling coefficient (η) associated with the out-of-plane current is smaller by a factor of 4. The experimental currents in the monodomain sample are in excellent agreement with the theoretical estimates of the shift current densities, which are 10.3 A/m and 13.3 A/m for the in-plane and out-of-plane components, respectively (see Supp. Info. for the details of the calculation). The consistency between the experimental current amplitudes and the first principle calculations shows an additional strong evidence that the photovoltaic effect in the monodomain BFO is governed by the bulk photovoltaic effect, i.e., shift current response. To compare the bulk shift current amplitudes to the DW-mediated currents, we consider the spatially localized nature of the currents associated with the DWs, and we estimate the peak DW-mediated current amplitude as $J_{DW}=40\frac{A}{m}\times\frac{1}{1.5\%}=2670\,A/m$, where 1.5% comes from the areal coverage of the DWs. Therefore, the current density associated with the charge separation at the DWs is more than two-orders of magnitude larger as compared to the bulk shift current response. This further highlights the importance of DWs providing nanoscale junctions for efficient charge separation underpinning the unique optoelectronic functionality observed in these photoferroic thin films.

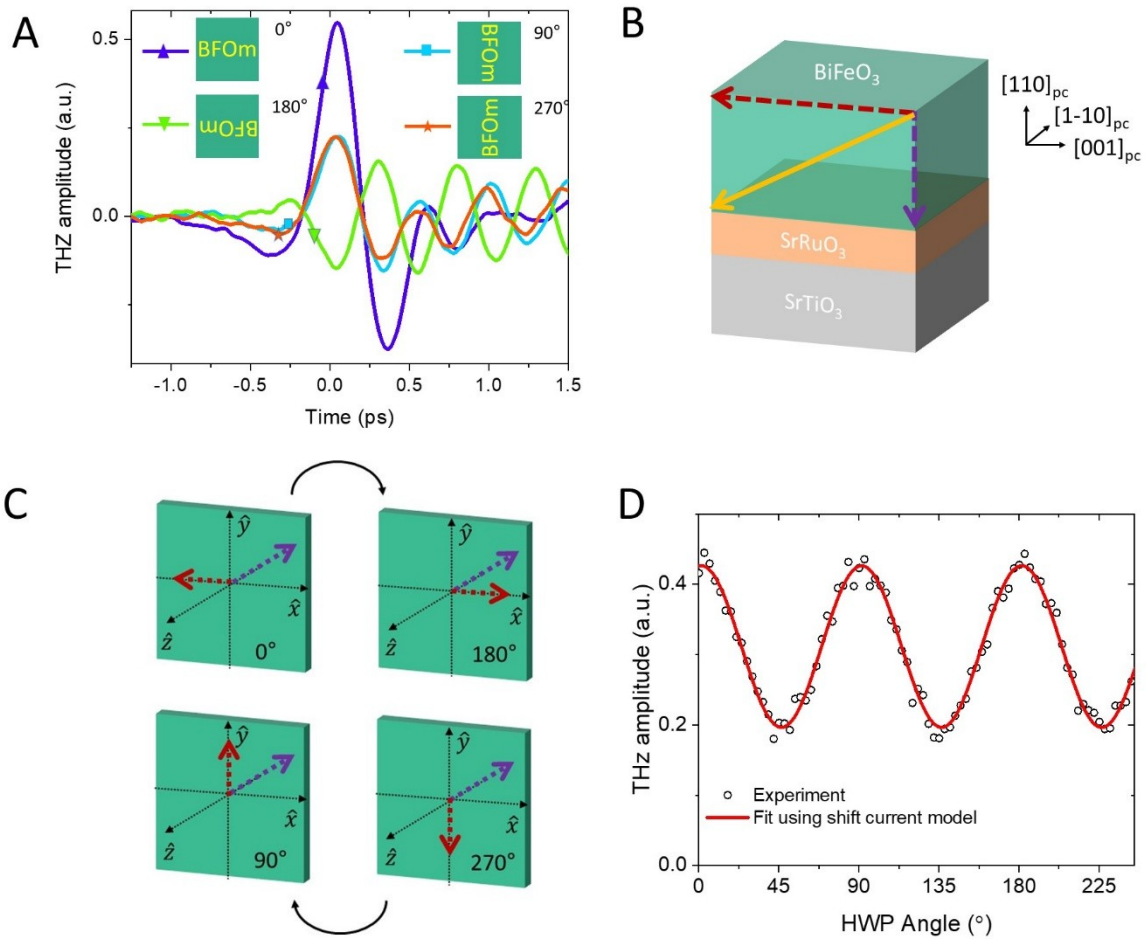

Figure 4. (a) Radiated THz transients for different azimuthal orientations of the monodomain $(110)_{pc}$ BFO sample. (b) Ferroelectric polarization with respect to the crystal axes in the monodomain BFO thin film. The in-plane and out-of-plane components are marked by red and purple arrows, respectively. (c) Depiction of the in-plane and out-of-plane ferroelectric polarizations for different azimuthal orientations of the monodomain sample. $[110]_{pc}$ and $[001]_{pc}$ point along $\hat{z}$ and $\hat{x}$, respectively. (d) Excitation light polarization dependence (half wave plate – HWP) of the emitted THz radiation from the monodomain BFO. The fit is performed using the shift current model described in the supporting information.

In summary, we disentangle and quantify the unique contributions of different photovoltaic mechanisms in epitaxial BFO films. In BFO with periodic stripe domains, domain-wall mediated charge separation is found to be the dominant mechanism, whereas a shift current response dominates in the case of monodomain BFO. We

show that light-induced currents are significantly stronger in BFO with stripe domains as compared to monodomain BFO due to the dominance of the domain-wall-mediated currents over the shift current response. Overall, BFO films with spontaneously-formed periodic stripes offer exciting prospects as bias-free THz emitters. Control of the domain wall density could enable practical broadband THz emitters based on ferroelectric materials.

Supporting information

THz emission spectroscopy setup, polarization analysis of the emitted THz radiation, calibration of the current directions, calculation of the peak THz field amplitude, calculation of the built-in fields at the domain walls, shift current calculations, piezo force microscopy images of the samples, growth procedures of the samples. This material is available free of charge via the Internet at http://pubs.acs.org.

Corresponding author

* Email: burakg@stanford.edu, aaronl@stanford.edu

Confilict of interest

The authors declare no financial competing financial interest.

Acknowledgments

The terahertz spectroscopy work was supported by the Department of Energy, Basic Energy Sciences, Materials Sciences and Engineering Division. L.Z. acknowledges support from the Army Research Office under Grant W911NF-14-1-0104. P.D. acknowledges support from the National Science Foundation under grant DMR-1708615. L.W.M. and A.L. acknowledges support from the U.S. Department of Energy, Office of Science, Office of Basic Energy Sciences, under Award Number DE-SC-0012375 for the study of ultrafast response of ferroic materials. A.B.M and D.G.S. acknowledge support from the Semiconductor Research Corporation (SRC) as nCORE task No. 2758.003 and the National Science Foundation (NSF) under the E2CDA (Grant No. ECCS 1740136) programs. Substrate preparation was performed in part at the Cornell NanoScale Facility, a member of the National Nanotechnology Coordinated Infrastructure (NNCI), which is supported by the NSF (Grant No. ECCS-1542081).

References

(1) *Ferroelectric materials for energy applications*; Huang, H., Scott, J. F., Eds.; Wiley-VCH Verlag.

(2) Martin, L. W.; Rappe, A. M. *Nat. Rev. Mater.* **2017**, *2* (2), 16087.

(3) Paillard, C.; Bai, X.; Infante, I. C.; Guennou, M.; Geneste, G.; Alexe, M.; Kreisel, J.; Dkhil, B. *Adv. Mater.* **2016**, *28* (26), 5153–5168.

(4) Fan, Z.; Sun, K.; Wang, J. *J. Mater. Chem. A* **2015**, *3* (37), 18809–18828.

(5) Kreisel, J.; Alexe, M.; Thomas, P. A. *Nat. Mater.* **2012**, *11* (4), 260–260.

(6) Seidel, J. *Nat. Mater.* **2019**, *18* (3), 188–190.

(7) Glass, A. M.; von der Linde, D.; Negran, T. J. *Appl. Phys. Lett.* **1974**, *25* (4), 233–235.

(8) Sturman, B. I.; Fridkin, V. M. *The photovoltaic and photorefractive effects in noncentrosymmetric materials*; Gordon and Breach Science Publishers, 1992.

(9) Agarwal, R.; Sharma, Y.; Chang, S.; Pitike, K. C.; Sohn, C.; Nakhmanson, S. M.; Takoudis, C. G.; Lee, H. N.; Tonelli, R.; Gardner, J.; Scott, J. F.; Katiyar, R. S.; Hong, S. *Phys. Rev. B* **2018**, *97* (5), 054109.

(10) Yang, S. Y.; Seidel, J.; Byrnes, S. J.; Shafer, P.; Yang, C.-H.; Rossell, M. D.; Yu, P.; Chu, Y.-H.; Scott, J. F.; Ager, J. W.; Martin, L. W.; Ramesh, R. *Nat. Nanotechnol.* **2010**, *5* (2), 143–147.

(11) Seidel, J.; Fu, D.; Yang, S.-Y.; Alarcón-Lladó, E.; Wu, J.; Ramesh, R.; Ager, J. W. *Phys. Rev. Lett.* **2011**, *107* (12), 126805.

(12) Bhatnagar, A.; Roy Chaudhuri, A.; Heon Kim, Y.; Hesse, D.; Alexe, M. *Nat. Commun.* **2013**, *4* (1), 2835.

(13) Matsuo, H.; Kitanaka, Y.; Inoue, R.; Noguchi, Y.; Miyayama, M.; Kiguchi, T.; Konno, T. J. *Phys. Rev. B* **2016**, *94* (21), 214111.

(14) Ji, W.; Yao, K.; Liang, Y. C. *Phys. Rev. B* **2011**, *84* (9), 094115.

(15) Yan, F.; Chen, G.; Lu, L.; Spanier, J. E. *ACS Nano* **2012**, *6* (3), 2353–2360.

(16) Young, S. M.; Zheng, F.; Rappe, A. M. *Phys. Rev. Lett.* **2012**, *109* (23), 236601.

(17) Butler, K. T.; Frost, J. M.; Walsh, A. *Energy Environ. Sci.* **2015**, *8* (3), 838–848.

(18) Pintilie, L.; Alexe, M. *J. Appl. Phys.* **2005**, *98* (12), 124103.

(19) Pintilie, L.; Dragoi, C.; Pintilie, I. *J. Appl. Phys.* **2011**, *110* (4), 044105.

(20) Lee, D.; Baek, S. H.; Kim, T. H.; Yoon, J.-G.; Folkman, C. M.; Eom, C. B.; Noh, T. W. *Phys. Rev. B* **2011**, *84* (12), 125305.

(21) Zhang, X. -C.; Hu, B. B.; Darrow, J. T.; Auston, D. H. *Appl. Phys. Lett.* **1990**, *56* (11), 1011–1013.

(22) Gu, P.; Tani, M. In *Terahertz Optoelectronics*; Springer-Verlag: Berlin/Heidelberg, 2005; pp 63–98.

(23) Guzelturk, B.; Belisle, R. A.; Smith, M. D.; Bruening, K.; Prasanna, R.; Yuan, Y.; Gopalan, V.; Tassone, C. J.; Karunadasa, H. I.; McGehee, M. D.; Lindenberg, A. M. *Adv. Mater.* **2018**, *30* (11), 1704737.

(24) Schmuttenmaer, C. A. *Chem. Rev.* **2004**, *104* (4), 1759–1780.

(25) Seifert, T.; Jaiswal, S.; Martens, U.; Hannegan, J.; Braun, L.; Maldonado, P.; Freimuth, F.; Kronenberg, A.; Henrizi, J.; Radu, I.; Beaurepaire, E.; Mokrousov, Y.; Oppeneer, P. M.; Jourdan, M.; Jakob, G.; Turchinovich, D.; Hayden, L. M.; Wolf, M.; Münzenberg, M.; Kläui, M.; Kampfrath, T. *Nat. Photonics* **2016**, *10* (7), 483–488.

(26) Sirica, N.; Tobey, R. I.; Zhao, L. X.; Chen, G. F.; Xu, B.; Yang, R.; Shen, B.; Yarotski, D. A.; Bowlan, P.; Trugman, S. A.; Zhu, J.-X.; Dai, Y. M.; Azad, A. K.; Ni, N.; Qiu, X. G.; Taylor, A. J.; Prasankumar, R. P. *Phys. Rev. Lett.* **2019**, *122* (19), 197401.

(27) Ma, E. Y.; Guzelturk, B.; Li, G.; Cao, L.; Shen, Z.-X.; Lindenberg, A. M.; Heinz, T. F. *Sci. Adv.* **2019**, *5* (2), eaau0073.

(28) Belinicher, V. I.; Sturman, B. I. *Sov. Phys. Uspekhi* **1980**, *23* (3), 199–223.

(29) Tan, L. Z.; Zheng, F.; Young, S. M.; Wang, F.; Liu, S.; Rappe, A. M. *npj Comput. Mater.* **2016**, *2* (1), 16026.

(30) Sipe, J. E.; Shkrebtii, A. I. *Phys. Rev. B* **2000**, *61* (8), 5337–5352.

(31) Cook, A. M.; M. Fregoso, B.; de Juan, F.; Coh, S.; Moore, J. E. *Nat. Commun.* **2017**, *8* (1), 14176.

(32) Rangel, T.; Fregoso, B. M.; Mendoza, B. S.; Morimoto, T.; Moore, J. E.; Neaton, J. B. *Phys. Rev. Lett.* **2017**, *119* (6), 067402.

(33) Chu, Y.-H.; He, Q.; Yang, C.-H.; Yu, P.; Martin, L. W.; Shafer, P.; Ramesh, R. *Nano Lett.* **2009**, *9* (4), 1726–1730.

(34) Shan, J.; Heinz, T. F. In *Ultrafast Dynamical Processes in Semiconductors*; Springer Berlin Heidelberg, 2004; pp 1–56.

(35) Beck, M.; Schäfer, H.; Klatt, G.; Demsar, J.; Winnerl, S.; Helm, M.; Dekorsy, T. *Opt. Express* **2010**, *18* (9), 9251.

(36) Mei, A. B.; Tang, Y.; Schubert, J.; Jena, D.; Xing, H. (Grace); Ralph, D. C.; Schlom, D. G. *APL Mater.* **2019**, *7* (7), 071101.

(37) Takahashi, K.; Kida, N.; Tonouchi, M. *Phys. Rev. Lett.* **2006**, *96* (11), 117402.

(38) Rana, D. S.; Kawayama, I.; Mavani, K.; Takahashi, K.; Murakami, H.; Tonouchi, M. *Adv. Mater.* **2009**, *21* (28), 2881–2885.

ToC image

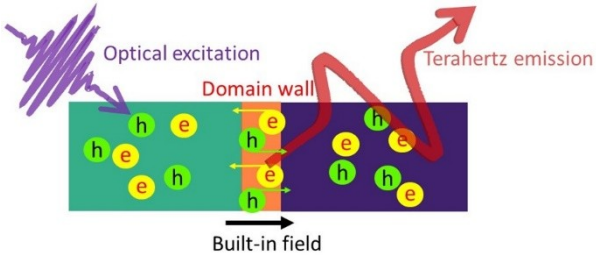
Optical excitation
Domain wall
Terahertz emission
Built-in field